ACS SENSORS

pubs.acs.org/acssensors

Article

Indolenine-Based Derivatives as Customizable Two-Photon Fluorescent Probes for pH Bioimaging in Living Cells

Carlos Benitez-Martin,[‖] Juan A. Guadix,[‖] John R. Pearson, Francisco Najera,* Jose M. Perez-Pomares,* and Ezequiel Perez-Inestrosa*

Cite This: *ACS Sens.* 2020, 5, 1068−1074

Read Online

ACCESS | Metrics & More | Article Recommendations | Supporting Information

ABSTRACT: Novel pH probes based on 2-(6-methoxynaphthalen-2-yl)-3,3-dimethyl-3H-indole have been synthesized and characterized. These compounds display excellent "off−on" fluorescence responses to acidic pH especially under two-photon (TP) excitation conditions as well as strong selectivity and sensitivity toward H^+. These features are supported by fluorescence quantum yields over 35%, TP cross sections ∼60 GM, and good resistance to photodegradation under acidic conditions. The synthetic versatility of this model allows subcellular targets to be tuned through minor scaffold modifications without affecting its optical characteristics. The effectiveness of the probes' innate photophysical properties and the structural modifications for different pH-related applications are demonstrated in mouse embryonic fibroblast cells.

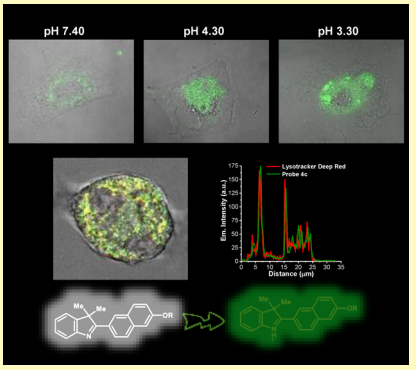

KEYWORDS: *intracellular pH, pH sensor, two-photon absorption, fluorescent probe, biosensor*

INTRODUCTION

Intracellular pH is an important aspect of biological processes whose accurate control underpins cellular and animal functions. Many processes, such as cellular proliferation and apoptosis,[1] enzymatic activity,[2] muscle contraction,[3] and ion transport,[4] are intimately related to pH. Likewise, the activity of many subcellular organelles depends on regulating their local pH. Lysosomes are recognized as the most acidic of all organelles. Their internal pH usually ranges from 4.5 to 5.0, with this being essential for their role in cellular homeostasis.[5] Abnormal pH severely affects the proper performance of most biological processes. Acidic pH is also commonly associated with diverse kinds of diseases, including cystic fibrosis,[6] Alzheimer's disease,[7] cancer,[8] and lysosomal storage disorders.[9] Thus, monitoring pH changes is a crucial part of following physiological and pathological processes. Fluorescence-based molecular imaging has emerged as a powerful technique for biological pH studies and clinical diagnosis, complementing, or even replacing, traditional methods such as nuclear magnetic resonance (NMR)[10] or microelectrodes.[11] Fluorescence imaging offers advantages ranging from operational simplicity, high sensitivity, and excellent temporal resolution to its noninvasiveness. These advantages can be further enhanced when combined with two-photon (TP) microscopy. TP microscopy uses the excitation window for biological imaging (700−1000 nm) that reduces scattering and absorption in organic samples. These near-infrared (NIR) excitation wavelengths also result in lower phototoxicity and lower biomacromolecule autofluorescence. To date, a wide variety of structural models has been devised for pH bioimaging, mainly focusing on one-photon (OP) probes.[12−14] Although some developments into TP pH sensors have been described recently,[14−28] there is still significant room for improvement in terms of designing effective TP fluorescent pH-sensitive probes. An overview of TP probes described so far in the literature is summarized in the Supporting Information. It is worth noting that the novel dyes reported here not only combine the necessary optical properties to act as acidic pH biosensors but also represent a new flexible dye platform. In contrast to other similar fluorophores, their scaffold can be easily adapted for other uses via straightforward modifications to their molecular architecture.

The recently reported TP-optimized hydroxyl radical sensor constitutes the starting point of this work.[29] Inspired by its molecular architecture, here we describe two pH (off/on) probes based on our previously prepared 2-(6-methoxynaphthalen-2-yl)-3,3-dimethyl-3H-indole. Although the acid−base properties of the indolenine ring have been studied in a recent pH sensor,[30] it was conceived and tested for OP microscopy.

Received: December 30, 2019
Accepted: March 31, 2020
Published: March 31, 2020

https://dx.doi.org/10.1021/acssensors.9b02590
ACS Sens. 2020, 5, 1068−1074

In this work, we have removed the π bridge between the donor and the acceptor units to avoid undesirable photochemical processes. Their structure was also specifically chosen to be optimal for biphotonic excitation. Under TP excitation conditions, the probes normally exist in a neutral non-fluorescent "off" state. However, upon conversion to a protonated "on" state, fluorescence can be readily detected under the same TP excitation conditions. The common scaffold displays a remarkable degree of synthetic versatility such that it can be modified for different applications without affecting its optical properties. The appropriate selection of substituents allows biological targeting to be effectively controlled, as confirmed by experiments using cultured cells, thus demonstrating the effectiveness of these probes for a range of pH bioimaging applications.

RESULTS AND DISCUSSION

Design and Synthesis of Compounds 4b,c. Indolenines **4a** and **4b** were prepared via the Fisher indole synthesis with phenylhydrazine hydrochloride and ketones **3a** and **3b**. These compounds (**3a**,**b**) were obtained from Williams' coupling reaction of the naphtol **2** with the corresponding dibromo or tosyl derivatives. Finally, the substitution of the bromo in **4a** with morpholine generated probe **4c** (Scheme 1). All

Scheme 1. Synthesis of Probes 4b,c

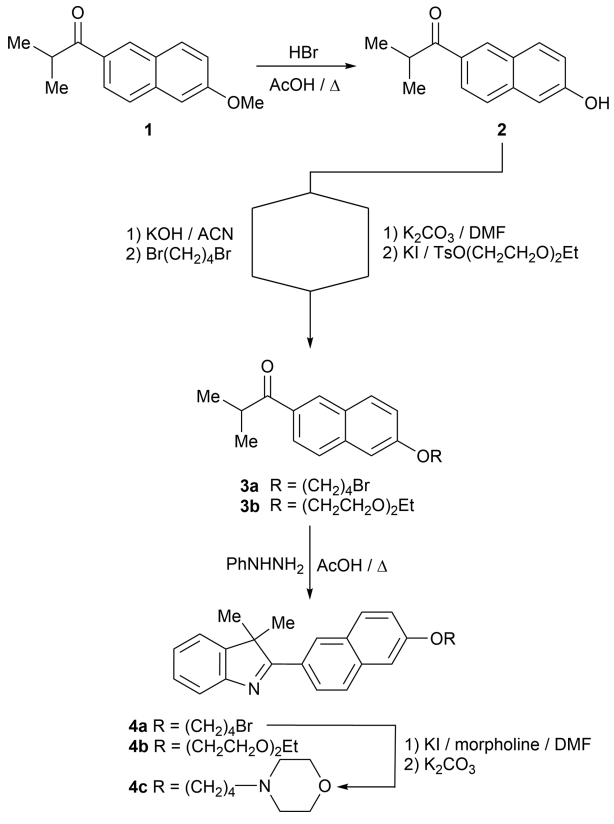

compounds were efficiently obtained in moderate to high yields (74−91%). All synthesized chemical structures were confirmed from their monodimensional and bidimensional NMR spectra and MS data (see the Supporting Information).

UV−Vis Absorption and Fluorescence Properties of Compounds 4b,c. The photophysical properties of compounds **4b,c** were fully characterized in terms of their absorption and emission spectra in different solvents (Table 1 and Figure S1 in the Supporting Information). Absorption maxima are located in a narrow wavelength interval between 332 and 338 nm with no significant influence from solvent polarity. In contrast, the fluorescence emission bands are greatly affected by this factor. Fluorescence maxima move from 412 to 438 nm into the blue-cyan spectral region, thus displaying a significant positive bathochromic effect. These solvatofluorochromic properties reveal a higher dipolar moment in the excited state in comparison to the ground state one. This solvent-dependent behavior also points to the presence of an ICT in these molecules. These properties are complemented by the combination of moderate fluorescence quantum yields (ca. 0.10−0.14) and a strong Stokes shift of up to 6790−6843 cm^{-1} (Table 1). Of particular interest is the absence of significant differences between the photophysical properties of these compounds, indicating that only the oxygen atom is involved in the push−pull system.

Optical Responses of Compounds 4b,c to pH and pKa Determination. Absorption and emission spectra were recorded in a hydrochloric acid solution (pH 1.22) (Table 1). As expected, nitrogen quaternization increases the electron-acceptor character of the indoliminium unit. This results in a more pronounced ICT character when the probes are protonated. This is demonstrated by the fact that the absorption bands are redshifted to approximately 400 nm for compounds **4b** + H^+ and **4c** + H^+. Emission band maxima are also redshifted to 500 nm, a displacement of ∼60 nm compared to their neutral forms.

Moreover, the improvement in the electron-withdrawing feature of the indolenine ring is associated with a remarkable fourfold increase in fluorescence quantum yields versus the neutral forms. This increase is accompanied with somewhat reduced Stokes shifts, although still exhibiting values of up to 4938 cm^{-1} (Table 1). The progressive bathochromic shift in the absorbance band when the solution turns acidic is shown in Figure 1a for compound **4b** (see Figure S2a in the Supporting Information for compound **4c**). This acid−base equilibrium is well illustrated by the sigmoidal fitting of absorbance with pH variation. Using the Henderson−Hasselbach mass-type equation, the pK_a was determined as 3.52 for both **4b** and **4c** (Table 1). Taking into account the fluorescence data (Figure 1b and Figure S2b in the Supporting Information), pK_a values were measured at 3.61 and 3.65, respectively. These results are consistent with previous studies into the acid−base properties of nitrogen heterocyclic compounds where no appreciable difference in the acidity character of the molecules is observed regardless of whether they are in ground or excited states.[31,32] Additionally, the absorption and emission properties of both probes exhibit good linearity in the range of pH 2.50−4.50.

To look deeper into the photophysics of these compounds, DFT and TD-DFT calculations were performed (see experimental details). As the alkoxy chain has no influence on the experimental photophysical properties, 2-(6-methoxynaphthalen-2-yl)-3,3-dimethyl-3H-indole was used as a reference model in the calculations.

In both neutral and protonated forms, the main electronic transition is $S_1 \leftarrow S_0$. This transition has a $\pi-\pi^*$ character and solely involves the HOMO and LUMO frontier orbitals (Table S1 and Figure S3 in the Supporting Information). In the neutral form, the HOMO is a π orbital while the LUMO is a π^* orbital with the electron density mainly located on the imine moiety. Protonation of the indolenine moiety improves

https://dx.doi.org/10.1021/acssensors.9b02590
ACS Sens. 2020, 5, 1068−1074

Table 1. Photophysical Properties of Compounds 4b,c (10 μM, Air Equilibrated Solutions) in Neutral and Acidic Conditions

compound	solvent	λ_{abs} (nm)[a]	λ_{em} (nm)[b]	ε_{max} (M^{-1} cm^{-1})	Stokes shift(cm^{-1})[c]	Φ_f (%)[d]	σ (GM)[e](800 nm)	pK_a (abs)	pK_a (em)
4b	THF	338	413	20,270	5373	1.3		3.52	3.61
	DCM	332	415	27,356	6024	1.7			
	MeOH	337	423	23,646	6033	2.2			
	H_2O	337	438	17,355	6843	9.9			
4b + H^+	HCl[f]	402	500	21,338	4876	34.9	57		
4c	THF	338	412	29,358	5314	2.2		3.52	3.65
	DCM	332	415	28,312	6024	3.3			
	MeOH	337	423	27,687	6033	3.2			
	H_2O	337	437	24,461	6790	14.0			
4c + H^+	HCl[f]	401	500	25,150	4938	40.8	61		

[a]Longest-wavelength absorption maximum. [b]Fluorescence emission maximum. [c]The Stokes shift as the difference between the maxima of the wavenumber-converted absorption and emission spectra. [d]Fluorescence emission quantum yield. [e]TP absorption cross sections measured at 800 nm. [f]HCl aqueous solution (0.06 M, pH 1.22).

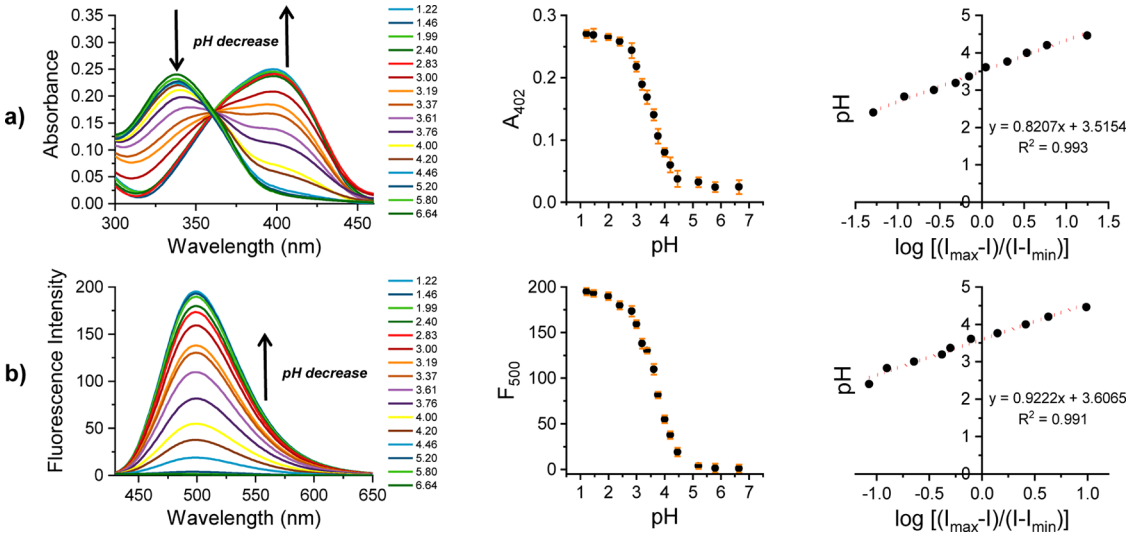

Figure 1. Absorption (row (a)) and emission (row (b)) spectra of compound **4b** at different pH values. Plot of absorbance (at 402 nm, row (a)) and emission (at 500 nm, row (b)) versus the pH value (mean of three independent experiments). Representation of the Henderson−Hasselbach mass equation for the absorbance (row (a)) and emission (row (b)) data. The pH was modified from 1.22 to 6.64.

the iminium's electron-withdrawing properties thus reducing HOMO electronic density on its carbon atom (Figure S3 in the Supporting Information). The LUMO now becomes a centered π^* orbital that is spread out over the iminium group. The energies of both the LUMO and HOMO are decreased in the protonated iminium versus the neutral imine. Band gap energies between these orbitals also become lower (Figure S3 in the Supporting Information), consistent with the redshift observed in the experimental absorption and emission spectra.

Proton Ion Sensing Mechanism. ^{1}H NMR was used to corroborate the connection between the changes in the photophysical properties and quaternization of the indolenine ring nitrogen. To this end, we performed a controlled addition of trifluoroacetic acid (TFA) to **4b,c** solutions and recorded the spectra.

Addition of 1 equiv of TFA to **4c** shifted the morpholine moiety signals downfield, confirming the higher basicity of the morpholine ring nitrogen (Figure 2). The addition of a second equivalent of acid yielded the iminium ion formation, and this addresses important deshielding effects in the aromatic region. Importantly, the signal of H_{1naph} is downfield-shifted from 8.61 to 8.75 ppm.

In addition to changes to the aromatic region, we found that the aliphatic part was also affected. The signal associated with the dimethyl protons was also greatly displaced from 1.64 to 1.73 ppm (Figure 2). The further addition of more TFA equivalents did not result in any changes to the spectra. In compound **4b**, only its aromatic region was affected by the addition of TFA, eliminating the possibility of other pH-sensitive positions. (Figure S4 in the Supporting Information).

Selectivity, Reversibility, and Photostability Studies. The selectivity of **4b** and **4c** toward H^+ over other physiologically important metal ions (Na^+, K^+, and Ca^{2+} among others) at pH 1.22 and 7.00 was tested. Our results found that only protons affect these compounds (Figure S5 in the Supporting Information), showing that these probes have a high specificity for this species.

This desirable feature is accompanied by an excellent reversible response to pH, displaying an almost negligible decrease in emission intensity (Figure S6 in the Supporting Information). Moreover, compounds **4b,c** exhibit strong photostability under neutral or acid conditions, maintaining their emission at 500 nm only in acidic environments. Further, the absence of appreciable emission in neutral conditions under continuous irradiation also corroborates the lack of photochemical processes that could disturb the photophysics of these compounds (Figure S7 in the Supporting Information).

https://dx.doi.org/10.1021/acssensors.9b02590
ACS Sens. 2020, 5, 1068−1074

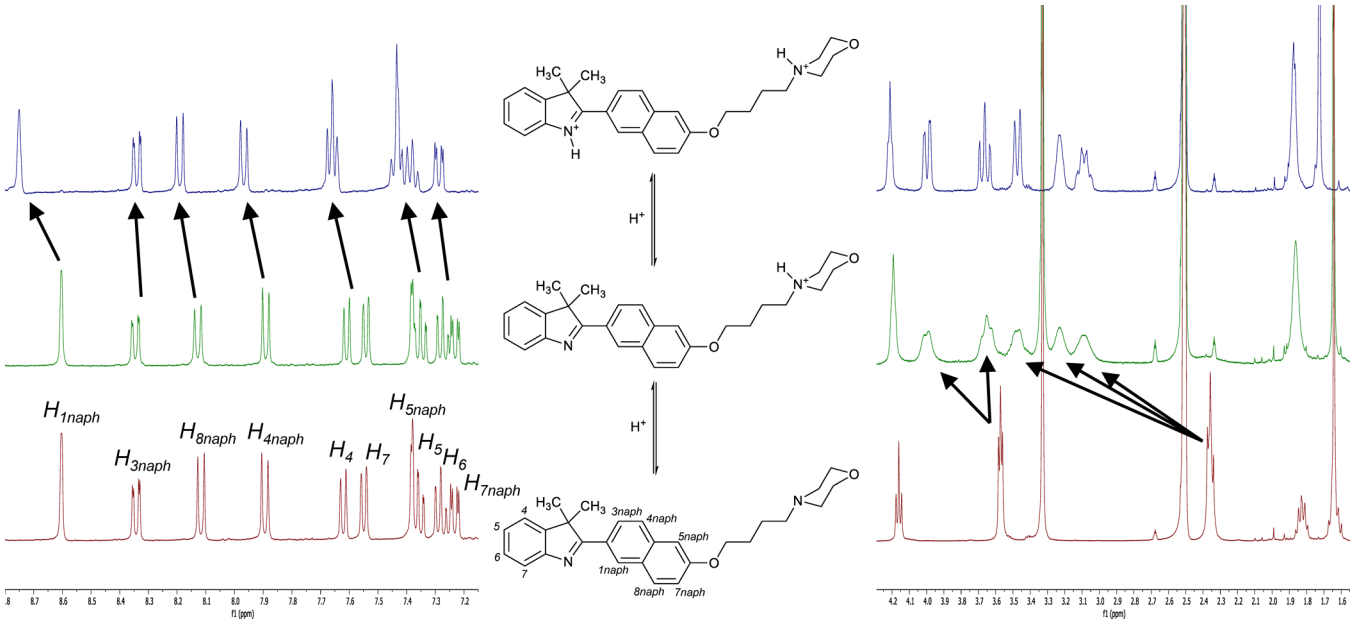

Figure 2. ^{1}H NMR spectra in DMSO-d_6 (aromatic and aliphatic regions) of probe **4c** before (lower row) and after the addition of 1 (middle row) and 2 equiv (upper row) of trifluoroacetic acid.

Two-Photon Absorption Properties. The absence of pronounced solvatochromic effects in the absorption bands of these compounds in their neutral forms precludes detection using the typical NIR wavelengths of TP microscopy.

However, when they are exposed to an acidic environment, an important bathochromic shift is observed in both their absorption and emission bands, as described above. This absorption band displacement is crucial for using these compounds with TP microscopy. Following the method of two-photon-induced fluorescence,[33] we investigated TP absorption properties between 700 and 1000 nm of these compounds. Considering the emission profile of the protonated dyes, excitation spectra were recorded, measuring fluorescence between 450 and 600 nm. The spectra for compounds **4b** and **4b** + H^+ (Figure 3a) reflect the off−on nature of these probes (see Figure S8 for compound **4c**). No emission was recorded from the off forms under biphotonic excitation, clearly indicating the protonated species (the on forms) as the TP-active derivatives. The energies of the excitation and emission processes in TP conditions point to S_1 and S_0 as the central characters of these transitions. The emission recorded by TP excitation displays a maximum at 505 nm for compounds **4b**,**c**. This value agrees with those obtained by OP excitation.

The cross sections of the protonated compounds were determined by comparison with rhodamine B as a reference, reaching values of ∼60 GM at 800 nm (Figure 3b). The linear relationship in the double-logarithmic plot of emission intensity versus laser power yields slopes of approximately 2.0, confirming the two-photon absorption event.

Two-Photon Fluorescence Cell Imaging. The toxicity of dyes **4b** and **4c** against mouse embryonic fibroblast cells (MEFs) was assessed using a WST-1 cell proliferation assay over 24 h. In both cases, the probes had no significant effect on cellular proliferation at concentrations of up to 10 μM (Figure S9 in the Supporting Information), indicating low cytotoxicity to MEFs.

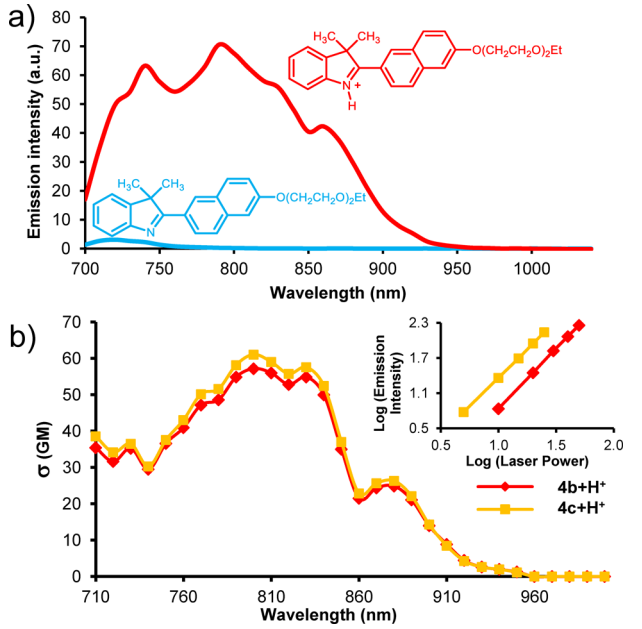

Figure 3. (a) TP excitation spectra of compounds **4d** (blue) and **4d** + H^+(red). (b) Protonated probe cross sections. Inset, upper-right, indicates the double-logarithmic plot of emission maximum intensity versus laser power. Slopes 1.9 and 1.8 were obtained for the indicated compounds.

To test the usefulness of **4b** and **4c** for live cell imaging, we performed TP microscopy experiments using MEF cells. Negative control cells, without **4b** or **4c**, did not show significant background fluorescence (see Figure S10 in the Supporting Information).

Probe **4b** was conceived as a general-purpose cellular pH probe without organelle-specific targeting. Its carbitol moiety was selected to aid solubility while allowing it to cross cellular membranes efficiently. This molecular architecture was designed to allow intracellular pH fluctuations to be followed by measuring changes in fluorescence. In a pH 7.40

https://dx.doi.org/10.1021/acssensors.9b02590
ACS Sens. 2020, 5, 1068−1074

environment, live **4b**-treated MEFs (Figure 4a,a′ and Figure S11a,a′) exhibited fluorescence at localized cytoplasmic

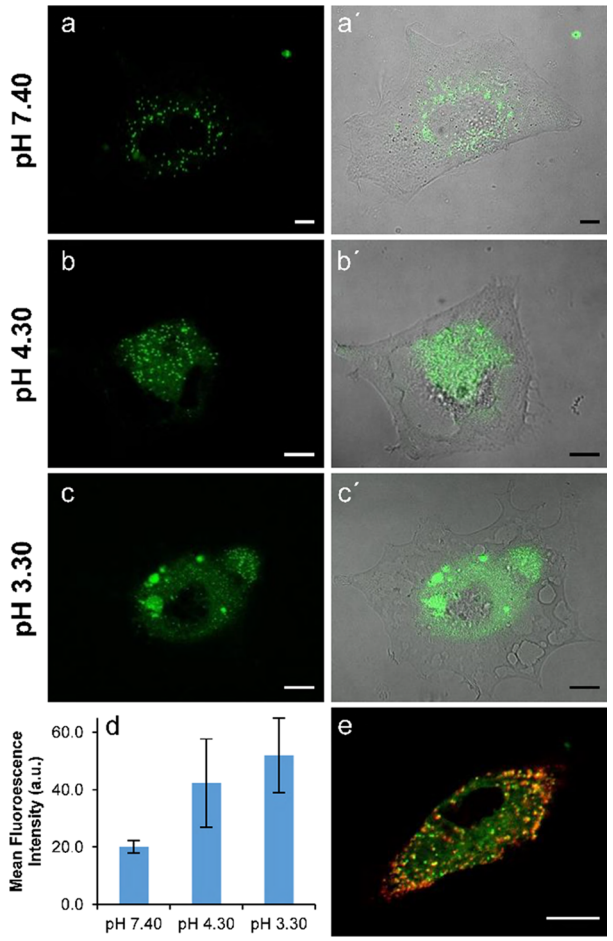

Figure 4. (a–c) Fluorescence images of probe **4b** (10^{-5} M, TP excitation: λ_{exc} = 800 nm, λ_{em} = 500–550 nm) and (a′–c′) merged with the brightfield in MEF cells at different pH values (7.4, 4.3, and 3.3). (d) Mean fluorescence intensity determined from six independent measures. (e) Colocalization-merged images at pH 4.3 of compound **4b** (green) and Lysotracker Deep Red (red). Intracellular pH was adjusted using a citrate/phosphate buffer and nigericin, as detailed in the Supporting Information. Scale bar: 10 μm

regions. Since acidic environments are required to convert the probes into their emissive forms under TP excitation, it suggests that the observed intracellular fluorescence occurred in acidic organelles, most likely lysosomes. Next, we used a treatment with nigericin and KCl to induce a global change in intracellular pH.[34,35] When pH decreased from 7.40 to 3.30, a gradual increase in cytoplasmic fluorescence was observed in parallel with the previously described cytoplasmic spots (Figure 4a–d and Figure S11a–c′). Treatment of MEF cells with a lysosome-specific probe (Lysotracker Deep Red) as a counterstain to **4b** (Figure 4e) at pH 4.3 suggests that almost all **4b** fluorescence colocalized with the lysosome-specific probe with appreciable signal in other cytoplasmic regions.

Tertiary amines are commonly considered lysosomotropic agents based on the acquisition of positive charge at a low pH.[36] As the inner membrane of the lysosome restricts the exchange of positively charged species, protonation results in their confinement inside these organelles.

We reasoned that the incorporation of a morpholine group in **4c** exerts a similar lysosome-anchoring activity. In contrast, the absence of this structural motif in **4b** should favor its diffusion throughout the cell. Thus, in contrast to **4b**, compound **4c** can be described as a "lysosensor". To test its lysosome-targeting ability, co-incubated cells were incubated at a physiological pH. As expected, bright green fluorescence was detected in discrete cytoplasmic regions after treatment with **4c** (Figure 5a). To corroborate the subcellular accumulation of

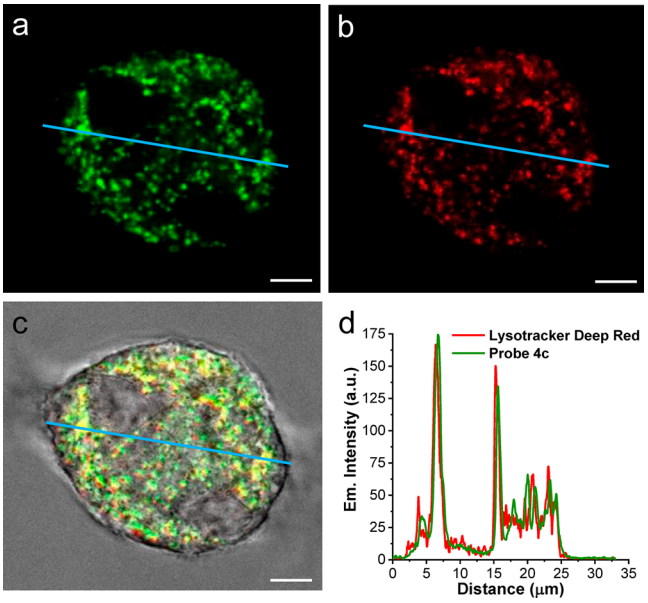

Figure 5. Colocalization images of MEF cells stained with (a) probe **4c** (10 μM, TP excitation: λ_{exc} = 800 nm, λ_{em} = 500–550 nm) and (b) Lysotracker Deep Red (50 nM, OP excitation: λ_{exc} = 633 nm, λ_{em} = 709–791 nm). (c) Colocalization-merged images: **4a**,**b** and brightfield. (d) Emission intensity profile plots along the blue lines of probe **4c** and Lysotracker Deep Red in MEF cells. Scale bar: 10 μm

this dye in living cells, Lysotracker Deep Red was again used (Figure 5b). The calculated Pearson correlation coefficient (PCC) for whole images was calculated at 0.84, showing good colocalization (see Figure S12 for experimental details). Moreover, excellent correlation was observed in emission intensity profiles, comparing probe intensity along linear regions of interest (blue line; Figure 5a–d). Importantly, the observed photophysics at the cellular level were fully consistent with the prior in vitro characterization of the protonated forms.

CONCLUSIONS

We have developed two novel pH-sensitive indolenine-based probes. These compounds show excellent photophysical properties that are significantly improved in acidic environments. In these conditions, fluorescence quantum yields of between 35 and 40% and a Stokes shift of around 4900 cm^{-1} are obtained. Moreover, the photophysical changes triggered by indolenine ring protonation allow its detection under TP excitation. Under these conditions, the neutral forms cannot be visualized, thereby constituting off–on probes and enhancing the signal-to-noise ratio. The protonated forms provided TP cross sections of up to 60 GM. In addition, these derivatives have good selectivity and sensitivity toward protons that are complemented by the reversibility of the modification, which greatly enhances their usefulness. As anticipated, changes to

https://dx.doi.org/10.1021/acssensors.9b02590
ACS Sens. 2020, 5, 1068–1074

the alkoxy moiety could be performed while maintaining their optical properties. We investigated our ability to control biological targeting using substituent exerts; whereas the nonspecific organelle-targeting probe **4b** can be used as a cytoplasmic pH sensor, the lysosome-targetable probe **4c** provided selective labelling of these organelles.

■ ASSOCIATED CONTENT

Supporting Information

The Supporting Information is available free of charge at https://pubs.acs.org/doi/10.1021/acssensors.9b02590.

Experimental data: chemical and instruments, synthesis, and characterization of the probes; DFT calculations; cell cultures; and two-photon microscopy studies (PDF)

■ AUTHOR INFORMATION

Corresponding Authors

Francisco Najera − *Departamento de Química Orgánica, Universidad de Málaga-IBIMA, Málaga 29071, Spain; Centro Andaluz de Nanomedicina y Biotecnología-BIONAND, Parque Tecnológico de Andalucía, Málaga 29071, Spain;* orcid.org/0000-0002-1635-5514; Email: najera@uma.es

Jose M. Perez-Pomares − *Departamento de Biología Animal, Facultad de Ciencias, Universidad de Málaga-IBIMA, Málaga 29071, Spain; Centro Andaluz de Nanomedicina y Biotecnología-BIONAND, Parque Tecnológico de Andalucía, Málaga 29071, Spain*; Email: jmperezp@uma.es

Ezequiel Perez-Inestrosa − *Departamento de Química Orgánica, Universidad de Málaga-IBIMA, Málaga 29071, Spain; Centro Andaluz de Nanomedicina y Biotecnología-BIONAND, Parque Tecnológico de Andalucía, Málaga 29071, Spain;* orcid.org/0000-0001-7546-5273; Email: inestrosa@uma.es

Authors

Carlos Benitez-Martin − *Departamento de Química Orgánica, Universidad de Málaga-IBIMA, Málaga 29071, Spain; Centro Andaluz de Nanomedicina y Biotecnología-BIONAND, Parque Tecnológico de Andalucía, Málaga 29071, Spain*

Juan A. Guadix − *Departamento de Biología Animal, Facultad de Ciencias, Universidad de Málaga-IBIMA, Málaga 29071, Spain; Centro Andaluz de Nanomedicina y Biotecnología-BIONAND, Parque Tecnológico de Andalucía, Málaga 29071, Spain*

John R. Pearson − *Centro Andaluz de Nanomedicina y Biotecnología-BIONAND, Parque Tecnológico de Andalucía, Málaga 29071, Spain*

Complete contact information is available at: https://pubs.acs.org/10.1021/acssensors.9b02590

Author Contributions

‖C.B-.M. and J.A.G. contributed equally.

Funding

This work was supported by the Spanish Ministerio de Ciencia, Innovación y Universidades (grants CTQ2016−75870-P, RTI2018−095410-BI00, RD16/0006/0012, and RD16/0011/0030), the Consejería de Salud, Junta de Andalucía (grants PI0250−2016 and PIER-0084-2019), Universidad de Málaga-Junta de Andalucía (UMA18-FEDERJA-007 and UMA18-FEDERJA-146), FEDER funds, and the FPU fellowship (FPU16/02516) for C.B-.M.

Notes

The authors declare no competing financial interest.

■ ACKNOWLEDGMENTS

We gratefully acknowledge the computer resources provided by the SCBI (Supercomputing and Bioinformatics Center) of the University of Malaga.

■ REFERENCES

(1) Lagadic-Gossmann, D.; Huc, L.; Lecureur, V. Alterations of Intracellular PH Homeostasis in Apoptosis: Origins and Roles. *Cell Death Differ.* **2004**, *11*, 953−961.

(2) Barott, K. L.; Barron, M. E.; Tresguerres, M. Identification of a Molecular PH Sensor in Coral. *Proc. R. Soc. B* **2017**, *284*, 20171769.

(3) Nogueira, L.; Shiah, A. A.; Gandra, P. G.; Hogan, M. C. Ca 2+ -Pumping Impairment during Repetitive Fatiguing Contractions in Single Myofibers: Role of Cross-Bridge Cycling. *Am. J. Physiol. Regul. Integr. Comp. Physiol.* **2013**, *305*, R118−R125.

(4) Delpiano, L.; Thomas, J. J.; Yates, A. R.; Rice, S. J.; Gray, M. A.; Saint-Criq, V. Esomeprazole Increases Airway Surface Liquid PH in Primary Cystic Fibrosis Epithelial Cells. *Front. Pharmacol.* **2018**, *9*, 1462.

(5) Gowrishankar, S.; Ferguson, S. M. Lysosomes Relax in the Cellular Suburbs. *J. Cell Biol.* **2016**, *212*, 617−619.

(6) Chen, J. H.; Xu, W.; Sheppard, D. N. Altering Intracellular PH Reveals the Kinetic Basis of Intraburst Gating in the CFTR Cl− Channel. *J. Physiol.* **2017**, *595*, 1059−1076.

(7) Fang, B.; Wang, D.; Huang, M.; Yu, G.; Li, H. Hypothesis on the Relationship between the Change in Intracellular PH and Incidence of Sporadic Alzheimer's Disease or Vascular Dementia. *Int. J. Neurosci.* **2010**, *120*, 591−595.

(8) Swietach, P.; Wigfield, S.; Cobden, P.; Supuran, C. T.; Harris, A. L.; Vaughan-Jones, R. D. Tumor-Associated Carbonic Anhydrase 9 Spatially Coordinates Intracellular PH in Three-Dimensional Multicellular Growths. *J. Biol. Chem.* **2008**, *283*, 20473−20483.

(9) Fukuda, T.; Ewan, L.; Bauer, M.; Mattaliano, R. J.; Zaal, K.; Ralston, E.; Plotz, P. H.; Raben, N. Dysfunction of Endocytic and Autophagic Pathways in a Lysosomal Storage Disease. *Ann. Neurol.* **2006**, *59*, 700−708.

(10) Taylor, J. S.; Deutsch, C. Fluorinated Alpha-Methylamino Acids as 19F NMR Indicators of Intracellular PH. *Biophys. J.* **1983**, *43*, 261−267.

(11) Caner, T.; Abdulnour-Nakhoul, S.; Brown, K.; Islam, M. T.; Hamm, L. L.; Nakhoul, N. L. Mechanisms of Ammonia and Ammonium Transport by Rhesus-Associated Glycoproteins. *Am. J. Physiol. Cell Physiol.* **2015**, *309*, C747−C758.

(12) Han, J.; Burgess, K. Fluorescent Indicators for Intracellular PH. *Chem. Rev.* **2010**, *110*, 2709−2728.

(13) Li, X.; Gao, X.; Shi, W.; Ma, H. Design Strategies for Water-Soluble Small Molecular Chromogenic and Fluorogenic Probes. *Chem. Rev.* **2014**, *114*, 590−659.

(14) Hou, J.-T.; Ren, W. X.; Li, K.; Seo, J.; Sharma, A.; Yu, X.-Q.; Kim, J. S.; Kikuchi, K.; DeBerardinis, R. J.; Gao, J.; et al. Fluorescent Bioimaging of PH: From Design to Applications. *Chem. Soc. Rev.* **2017**, *46*, 2076−2090.

(15) Lim, C. S.; Cho, B. R. Two-Photon Probes for Biomedical Imaging. *Tetrahedron* **2015**, *71*, 8219−8249.

(16) Han, Z.; Tan, J.; Wei, T.; Zhang, Y.; Xiao, H.; Xu, L.; He, B. Two Novel Two-Photon Fluorescent Probes for Low PH Values and Cell Imaging Based on Spirobifluorene Motif. *Sens. Actuators, B* **2018**, *255*, 2290−2297.

(17) Lu, X.; Zhang, G.; Li, D.; Tian, X.; Ma, W.; Li, S.; Zhang, Q.; Zhou, H.; Wu, J.; Tian, Y. Thiophene Aromatic Amine Derivatives with Two-Photon Activities as Probes for the Detection of Picric Acid and PH. *Dyes and Pigments* **2019**, *170*, 107641.

(18) Zhang, T.; Xu, D.; Poon, C. Y.; Wang, X.; Bolze, F.; Li, H. W.; Wong, M. S. Tuning the PK_a of Two-Photon Bis-Chromophoric

Probes for Ratiometric Fluorescence Imaging of Acidic PH in Lysosomes. *Talanta* **2019**, *202*, 34−41.
(19) Wang, F.; Liu, D.; Shen, Y.; Liu, J.; Li, D.; Tian, X.; Zhang, Q.; Wu, J.; Li, S.; Tian, Y. A Two-Photon Mitochondria-Targeted Fluorescent Probe for the Detection of PH Fluctuation in Tumor and Living Cells. *Dyes Pigm.* **2019**, *166*, 92−97.
(20) Jiang, X.; Liu, Z.; Yang, Y.; Li, H.; Qi, X.; Ren, W. X.; Deng, M.; Lü, M.; Wu, J.; Liang, S. A Mitochondria-Targeted Two-Photon Fluorescent Probe for Sensing and Imaging PH Changes in Living Cells. *Spectrochim. Acta, Part A* **2020**, *224*, 117435.
(21) Kim, H. M.; Cho, B. R. Small-Molecule Two-Photon Probes for Bioimaging Applications. *Chem. Rev.* **2015**, *115*, 5014−5055.
(22) Chen, S.; Zhao, M.; Su, J.; Zhang, Q.; Tian, X.; Li, S.; Zhou, H.; Wu, J.; Tian, Y. Two Novel Two-Photon Excited Fluorescent PH Probes Based on the A-π-D-π-A System for Intracellular PH Mapping. *Dyes Pigm.* **2017**, *136*, 807−816.
(23) Luo, W.; Jiang, H.; Tang, X.; Liu, W. A Reversible Ratiometric Two-Photon Lysosome-Targeted Probe for Real-Time Monitoring of PH Changes in Living Cells. *J. Mater. Chem. B* **2017**, *5*, 4768−4773.
(24) Dong, B.; Song, X.; Kong, X.; Wang, C.; Zhang, N.; Lin, W. A Tumor-Targeting and Lysosome-Specific Two-Photon Fluorescent Probe for Imaging PH Changes in Living Cells. *J. Mater. Chem. B* **2017**, *5*, 988−995.
(25) Ma, J.; Li, W.; Li, J.; Shi, R.; Yin, G.; Wang, R. A Small Molecular PH-Dependent Fluorescent Probe for Cancer Cell Imaging in Living Cell. *Talanta* **2018**, *182*, 464−469.
(26) Xu, D.; Li, Y.; Poon, C.-Y.; Chan, H.-N.; Li, H.-W.; Wong, M. S. A Zero Cross-Talk Ratiometric Two-Photon Probe for Imaging of Acid PH in Living Cells and Tissues and Early Detection of Tumor in Mouse Model. *Anal. Chem.* **2018**, *90*, 8800−8806.
(27) Ning, P.; Hou, L.; Feng, Y.; Xu, G.; Bai, Y.; Yu, H.; Meng, X. Real-Time Visualization of Autophagy by Monitoring the Fluctuation of Lysosomal PH with a Ratiometric Two-Photon Fluorescent Probe. *Chem. Commun.* **2019**, *55*, 1782−1785.
(28) Dou, Y.; Kenry, K.; Liu, J.; Zhang, F.; Cai, C.; Zhu, Q. 2-Styrylquinoline-Based Two-Photon AIEgens for Dual Monitoring of PH and Viscosity in Living Cells. *J. Mater. Chem. B* **2019**, *7*, 7771−7775.
(29) Benitez-Martin, C.; Guadix, J. A.; Pearson, J. R.; Najera, F.; Perez-Pomares, J. M.; Perez-Inestrosa, E. A Turn-on Two-Photon Fluorescent Probe for Detecting Lysosomal Hydroxyl Radicals in Living Cells. *Sens. Actuators, B* **2019**, *284*, 744−750.
(30) Niu, W.; Wei, Z.; Jia, J.; Shuang, S.; Dong, C.; Yun, K. A Ratiometric Emission NIR-Fluorescent Probe for Sensing and Imaging PH Changes in Live Cells. *Dyes Pigm.* **2018**, *152*, 155−160.
(31) Rosenberg, L. S.; Simons, J.; Schulmans, S. G. Determination of PKa Values of N-Heterocyclic Bases by Fluorescence Spectrophotometry. *Talanta* **1979**, *26*, 867−871.
(32) Berezin, M. Y.; Kao, J.; Achilefu, S. PH-Dependent Optical Properties of Synthetic Fluorescent Imidazoles. *Chem. - A Eur. J.* **2009**, *15*, 3560−3566.
(33) Terenziani, F.; Katan, C.; Badaeva, E.; Tretiak, S.; Blanchara-Desce, M. Enhanced Two-Photon Absorption of Organic Chromophores: Theoretical and Experimental Assessments. *Adv. Mater.* **2008**, *20*, 4641−4678.
(34) Ohkuma, S.; Moriyama, Y.; Takano, T. Identification and Characterization of a Proton Pump on Lysosomes by Fluorescein-Isothiocyanate-Dextran Fluorescence. *Proc. Natl. Acad. Sci. U. S. A.* **1982**, *79*, 2758−2762.
(35) Richardson, D. S.; Gregor, C.; Winter, F. R.; Urban, N. T.; Sahl, S. J.; Willig, K. I.; Hell, S. W. SRpHi Ratiometric PH Biosensors for Super-Resolution Microscopy. *Nat. Commun.* **2017**, *8*, 577.
(36) Xu, W.; Zeng, Z.; Jiang, J. H.; Chang, Y. T.; Yuan, L. Discerning the Chemistry in Individual Organelles with Small-Molecule Fluorescent Probes. *Angew. Chem., Int. Ed.* **2016**, *55*, 13658−13699.

https://dx.doi.org/10.1021/acssensors.9b02590
ACS Sens. 2020, 5, 1068−1074